# Global Land-Based Datasets for Monitoring Climatic Extremes

BY M.G. DONAT, L.V. ALEXANDER, H. YANG, I. DURRE, R. VOSE, J. CAESAR

F or more than a decade, the World Meteorological Organization (WMO) Commission for Climatology (CCl)/CLIVAR/JCOMM Expert Team on Climate Change Detection and Indices (ETCCDI) has been facilitating the international coordination of a suite of indices that primarily represent the more extreme aspects of climate. The main aim of this team has been to fill in data gaps using a consistent and traceable approach in order to provide a clear global picture of the long-term variability of extremes, to provide the necessary data to perform appropriate "detection and attribution" studies, and to be able to evaluate climate models and assess their efficacy in simulating and projecting the future of climate extremes. To this end, the ETCCDI held a number of regional workshops over many years, the data from which were used to help create HadEX, the first global land-based, gridded dataset of temperature and precipitation extremes covering the second half of the twentieth century.

While HadEX facilitated the analysis of trends in extremes, its relatively short record (1951–2003) and static nature (i.e., it is not updated) presents critical gaps in our ability to adequately assess and monitor changes in extremes. Furthermore, much of the data from the regional workshops is not publically available, making it difficult to independently reproduce

the results of HadEX. For these reasons, the authors set out to develop a new dataset to address these issues using the world's largest repository of daily in situ observations of temperature and precipitation—the National Climatic Data Center (NCDC)'s Global Historical Climatology Network (GHCN)-Daily dataset. This article describes the resulting dataset, termed GHCNDEX—an operationally updated, global land gridded dataset of climate extremes. We also demonstrate the application of the dataset for climate change and climate monitoring purposes in addition to assessing some issues regarding uncertainty by comparing the results with existing datasets.

**OBSERVATIONAL DATA.** GHCN-Daily is the premier source of daily observations of maximum and minimum temperatures as well as daily precipitation amounts from various regions of the globe. The dataset is composed of observations from numerous data sources that have been integrated and undergone extensive quality assurance reviews. As of October 2012, GHCN-Daily contains roughly 29,000 stations with daily maximum and minimum temperature and more than 80,000 stations with daily precipitation amounts (version 3.00-upd-2012100507—see Fig. 1a,c,e). Although the database is updated regularly over Europe, North America, and Australia as well as at several hundred synoptic stations across numerous countries, many records from Asia, Africa, and South America do not contain data from the most recent years. In addition, while many records are short or incomplete, many others—especially in North America, Europe, and Australia—date back well into the nineteenth century. At present, there are no bias adjustments available for GHCN-Daily to account for historical changes in instrumentation, observing practice, station location, or site conditions.

**CLIMATE INDICES ON GLOBAL GRIDS.**
GHCNDEX contains 26 of the indices recommended by the ETCCDI (see Table 1). Of these, 16 are temper-

**AFFILIATIONS:** DONAT, ALEXANDER, AND YANG—Climate Change Research Centre, and ARC Centre of Excellence for Climate System Science, University of New South Wales, Sydney, Australia; DURRE AND VOSE—NOAA's National Climatic Data Center, Asheville, North Carolina; CAESAR—Met Office Hadley Centre, Exeter, United Kingdom
**CORRESPONDING AUTHOR:** Markus Donat, Climate Change Research Centre, University of New South Wales, Sydney, Australia
E-mail: m.donat@unsw.edu.au

(a) Tmax 29277 stations

(b) TXx 40+years 5008 stations

(c) Tmin 29173 stations

(d) TNn 40+years 4798 stations

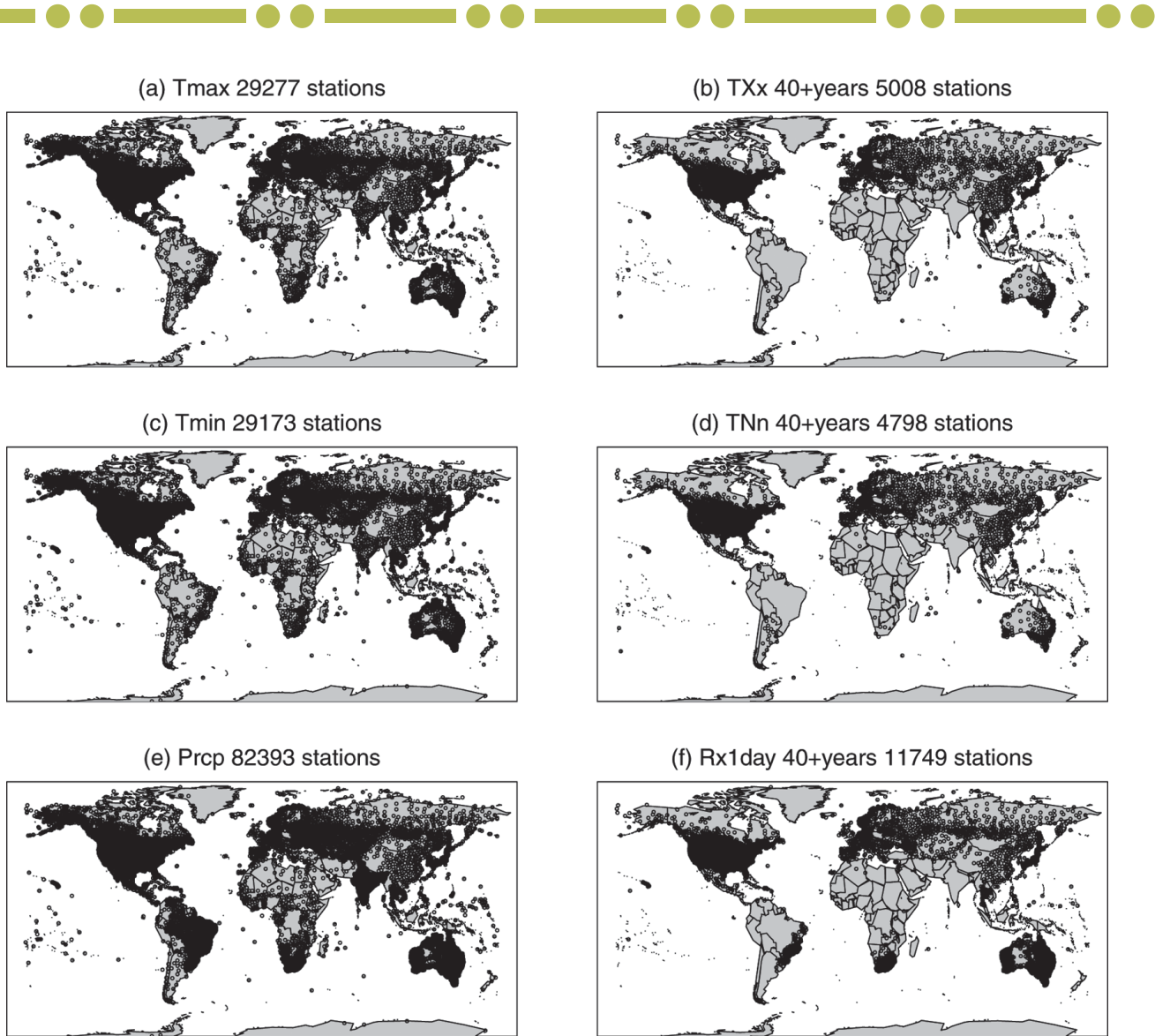(e) Prcp 82393 stations

(f) Rx1day 40+years 11749 stations

**Fɪɢ. 1. Locations of station observations in the GHCN-Daily archive. Left-hand side: All stations which provide daily data to calculate the climate indices based on (a) Tmax, (c) Tmin, (e) precipitation. Right-hand side: Stations which provide at least 40 years of calculated index data—for example, (b) TXx based on Tmax, (d) TNn based on Tmin, and (f) Rx1day based on daily precipitation amounts (see Table 1).**

ature-based and 10 are precipitation-based. Table 1 also notes which indices are calculated monthly and annually (e.g., hottest/wettest day, coldest night) and which only produce one value per year (e.g., frost day frequency, precipitation intensity). Most of the indices themselves are intended to measure some of the more extreme aspects of climate, characterizing the intensity, duration, or frequency of various climate events.

Each of the 26 indices is computed separately for each station. The station-based indices are then averaged together in a manner that accounts for their uneven distribution in space and time, minimizing

data quality issues at individual stations, and facilitating comparisons with climate model output. In particular, global gridded fields, with a grid box size of 2.5° of latitude by 2.5° of longitude, are calculated for each climate index over land surface areas (note that the grid box area varies for different latitudes: at the equator, a grid box covers an area of approximately 275 × 275 km, with smaller grid box sizes at higher latitudes). To create gridded values, spatial interpolation of the station-based indices is performed using an algorithm that considers the underlying spatial correlation structure of the data, a modified

version of Shepard's angular distance weighting (Shepard 1968; see Alexander et al. 2006 for details).

While indices are calculated for the stations' full period of record, we only calculate gridded fields from 1951 onward since coverage is reasonably good over most of the land areas of the globe after 1950. Also, to help minimize the effect of varying station density, we only use stations with at least 40 years of valid data after 1950 (see Fig. 1b,d,f). This step reduces the number of stations used for gridding by a factor of six or seven. For example, we keep roughly 5,000 temperature stations for gridding the warmest maximum temperature (TXx), and about 12,000 precipitation stations for gridding the maximum one-day precipitation total (Rx1day).

GHCNDEX generally compares well with other observation-based datasets of climate extremes, such as HadEX (Alexander et al. 2006) and temperature extremes calculated from HadGHCND (Caesar et al. 2006), a daily gridded temperature dataset that also uses GHCN-Daily as input (Fig. 2). For the precipitation indices, the agreement with HadEX is somewhat less robust, but this is almost entirely a function of the underlying source data (and thus spatial coverage); masking HadEX to the sparser coverage provided by GHCNDEX (dashed line in Fig. 2e) significantly increases the agreement between the
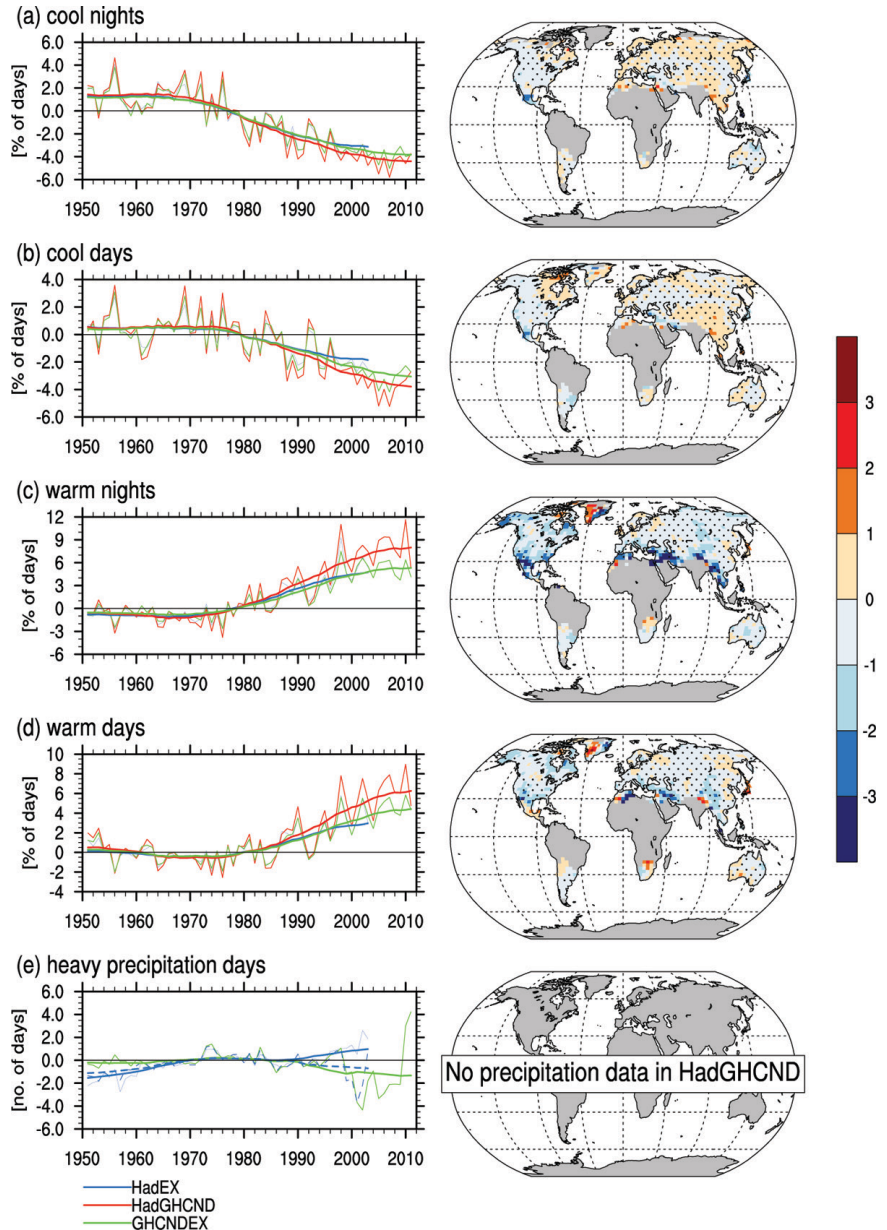


**Fig. 2. Global average time series (left) for the different datasets and (right) difference maps showing GHCNDEX minus HadGHCND for selected extremes indices. Annual values (thin lines) and 21-yr Gaussian filtered values (thick lines) are shown as anomalies from the respective 1961–90 average. For comparison, global average time series from HadEX (data period 1951–2003) are also included. Solid lines represent the area-weighted average in each dataset of all available grid boxes with at least 40 years of data, the blue dashed line in (e) shows the average of HadEX grid boxes masked to where GHCNDEX contains valid data. Difference maps use the 60-yr period 1951–2010, stippling indicates local Spearman rank correlation coefficients above 0.8. Note that for all grid boxes, differences are not significant at the 5% level (Kolmogorov-Smirnov-Test). For comparison, GHCNDEX was interpolated to the 3.75° x 2.5° grid used by HadGHCND and HadEX. Units as indicated in Table 1.**

**TABLE 1. List of the temperature and precipitation indices recommended by the ETCCDI and calculated for this study based on GHCN-Daily station data (index based on a user-defined threshold is omitted). Percentile values used as threshold for some of the indices are calculated for the base period 1961–90. See http://etccdi .pacificclimate.org/list_27_indices.shtml for exact definitions. A " * " indicates indices with monthly and annual output intervals; all other indices provide only annual output. Decadal trend estimates of global averages are also shown for the annual index values, significant trends (p ≤ 0.05, Mann-Kendall test) are indicated in bold. Only grid boxes with at least 40 years of data are used for the global average calculation.**

| Index | (A) Temperature _Intensity_ | Definition | Unit | Decadal trend: 1951–2011 _GHCNDEX_ | _HadGHCND_ |
|-------|------------------|------------|------|---------|----------|
| TXn* | Min Tmax | Coldest daily maximum temperature | °C | **0.28** | **0.27** |
| TNn* | Min Tmin | Coldest daily minimum temperature | °C | **0.45** | **0.39** |
| TXx* | Max Tmax | Warmest daily maximum temperature | °C | **0.11** | **0.10** |
| TNx* | Max Tmin | Warmest daily minimum temperature | °C | **0.12** | **0.17** |
| DTR* | Diurnal temperature range | Mean difference between daily maximum and daily minimum temperature | °C | **−0.09** | **−0.06** |
| | _Duration_ | | | | |
| GSL | Growing season length | Annual number of days between the first occurrence of 6 consecutive days with Tmean > 5°C and first occurrence of consecutive 6 days with Tmean < 5°C. For the Northern Hemisphere, this is calculated from 1 Jan to 31 Dec while for the Southern Hemisphere it is calculated from 1 Jul to 30 Jun. | days | **1.01** | **1.25** |
| CSDI | Cold spell duration indicator | Annual number of days with at least 6 consecutive days when Tmin < 10th percentile | days | **−0.62** | **−1.03** |
| WSDI | Warm spell duration indicator | Annual number of days with at least 6 consecutive days when Tmax > 90th percentile | days | **1.18** | **2.37** |
| | _Frequency_ | | | | |
| TX10p* | Cool days | Share of days when Tmax < 10th percentile | % of days | **−0.67** | **−0.86** |
| TN10p* | Cool nights | Share of days when Tmin < 10th percentile | % of days | **−1.09** | **−1.26** |
| TX90p* | Warm days | Share of days when Tmax > 90th percentile | % of days | **0.80** | **1.14** |
| TN90p* | Warm nights | Share of days when Tmin > 90th percentile | % of days | **1.17** | **1.79** |
| FD | Frost days | Annual number of days when Tmin < 0°C | days | **−1.80** | **−1.72** |

| Index | (A) Temperature _Frequency_ | Definition | Unit | Decadal trend: 1951–2011 | |
|---|---|---|---|---|---|
| ID | Icing days | Annual number of days when Tmax < 0°C | days | **−1.23** | **−1.18** |
| SU | Summer days | Annual number of days when Tmax > 25°C | days | **0.47** | 0.54 |
| TR | Tropical nights | Annual number of days when Tmin > 20°C | days | **0.91** | **1.05** |
| | **(B) Precipitation** _Intensity_ | | | | |
| Rx1day* | Max 1-day precipitation | Maximum 1-day precipitation total | mm | 0.04 | N/A |
| Rx5day* | Max 5-day precipitation | Maximum 5-day precipitation total | mm | −0.31 | N/A |
| SDII | Simple daily intensity index | Annual total precipitation divided by the number of wet days (i.e., when precipitation ≥ 1.0 mm) | mm/day | **−0.07** | N/A |
| R95p | Annual contribution from very wet days | Annual sum of daily precipitation > 95th percentile | mm | **1.98** | N/A |
| R99p | Annual contribution from extremely wet days | Annual sum of daily precipitation > 99th percentile | mm | **1.42** | N/A |
| PRCPTOT | Annual contribution from wet days | Annual total precipitation from days ≥ 1 mm | mm | 0.23 | N/A |
| | _Duration_ | | | | |
| CWD | Consecutive wet days | Maximum annual number of consecutive wet days (i.e., when precipitation ≥ 1 mm) | days | 0.02 | N/A |
| CDD | Consecutive dry days | Maximum annual number of consecutive dry days (i.e., when precipitation < 1 mm) | days | **−1.66** | N/A |
| | _Frequency_ | | | | |
| R10mm | Heavy precipitation days | Annual number of days when precipitation ≥ 10 mm | days | −0.07 | N/A |
| R20mm | Very heavy precipitation days | Annual number of days when precipitation ≥ 20 mm | days | −0.03 | N/A |

globally averaged indices from both datasets. This also shows that spatial coverage is one of the major sources of uncertainty when calculating global trends, particularly for the precipitation indices whose changes are spatially more complex, and thus global changes are more sensitive to regional coverage. As already noted, the spatial coverage of HadEX is more complete because it incorporated data collected from a number of regional workshops. In these cases, only climate indices were provided for these regions and thus the daily data are not available via the GHCN-Daily archive. Therefore, we recommend that appropriate masks for data completeness should be applied when analyzing time series of area averages.

The comparison with indices derived from HadGHCND allows us to learn about the sensitivity of the results to two different computational approaches: the GHCNDEX approach of gridding indices computed from station data and the alternative approach (in this case using HadGHCND) of first gridding daily station observations and then computing indices from those gridded fields. This comparison is of particular interest because indices from climate model simulations, for example, are also calculated from daily gridded fields, and it remains to be determined to what extent indices computed in this way are comparable to datasets that interpolate grids of the extremes indices calculated at station locations. Figure 2 shows some regional differences in absolute values between GHCNDEX and HadGHCND, although the null hypothesis that data are drawn from the same distribution can generally not be rejected at the 5% level (Kolmogorov–Smirnov test). Particularly for the frequencies of warm days and warm nights (Fig. 2c,d), the 60-year average is somewhat larger in HadGHCND compared to GHCNDEX, and this is related to a stronger increase in these indices after around 1980 in HadGHCND. For the indices defined as absolute temperature values, there are some systematic differences, with monthly and annual maximum values (e.g., TXx, TNx) being generally higher in GHCNDEX than in HadGHCND, whereas minimum values (e.g., TXn, TNn) tend to be lower in GHCNDEX (not shown). Despite biases in absolute values, the local correlations of indices from GHCNDEX and HadGHCND are generally high (greater than 0.8 using Spearman's rank) and significant at almost all grid boxes. Some larger differences between both datasets are found around 30°N [e.g., HadGHCND has fewer warm nights than GHCNDEX (see Fig. 2c)], and this also coincides with a lower correlation (although still significant) between the datasets.

**TRENDS IN CLIMATE EXTREMES.** To highlight the usefulness of these index datasets, we show time series and trends from a selection of the gridded products from 1951 to 2011 (see Figs. 2, 3). For comparison, we additionally show trends of temperature indices based on HadGHCND, and we also compare with global average time series from HadEX. Linear trends are calculated here using Sen's trend estimator (Sen 1968) and trend significance is estimated using the Mann-Kendall test (Kendall 1975). These meth-ods do not make assumptions about the underlying distribution, and this is particularly important for the precipitation extremes, which do not necessarily follow a Gaussian distribution.

In general, the temperature-related indices display warming trends during the past 60 years over most of the land areas covered in this study, with generally stronger increases in minimum temperature than in maximum temperature. Most significantly, the frequency of cool nights is found to have decreased significantly during the past 60 years over almost all covered land areas (Fig. 3a), with the converse generally being true for warm nights (Fig. 3c). The frequencies of warm days and cool days also show clear warming trends over large areas (Fig. 3b,d). However, in some regions cooling is found in temperature extremes. In particular, the maximum-temperature-related indices (such as the frequency of warm days, Fig. 3d) also show the apparent "warming hole" over eastern North America, displaying a regional (generally not significant) cooling trend that is also obvious from average temperatures. In some regions, the warming trends seem to be stronger in HadGHCND than in GHCNDEX—for example, over large parts of Eurasia as reflected by the frequency of cold days and warm days (Fig. 3b,d). This also explains the stronger warming of the global average in HadGHCND (Fig. 2). Note that for some regions outside of Europe, North America, and Australia, Fig. 3 does not show actual 60-year trends, due to limited availability of recent observations. However, for most regions shown, the trends represent changes during 50+ years after 1951.

Changes in precipitation extremes are spatially less consistent compared to the dominant warming observed in the temperature indices over the last 60 years, and are also mostly less significant. Many of the precipitation indices consistently indicate (in some cases significant) increases in precipitation extremes over eastern North America, eastern Europe and Scandinavia, tropical northern Australia, and Brazil (e.g., Figure 3e for heavy precipitation days). Generally nonsignificant drying trends are reflected in the precipitation extremes indices over eastern Asia, northwestern North America, southwest Europe, and some regions in eastern and southwestern Australia. On average, over the global land areas with data, some of the precipitation indices display slight trends toward wetter conditions (see Table 1), such as significant increases in precipitation amounts above the 95th and 99th percentiles.

## UTILITY FOR CLIMATE MONITORING.

A key purpose of GHCNDEX is as an operational monitoring product for extreme climatic events related to temperature and precipitation. This not only allows us to see the magnitude and extent of extreme events in near-real time, but also to place them in the context of longer-term changes at both global and regional scales. An additional advantage is the ability to view analogous changes in minimum and maximum temperature and precipitation extremes. To demonstrate the suitability of the gridded climate indices for climate monitoring applications, here we present three different events affecting different regions in the recent past characterized by particularly warm or cool and wet conditions.

*Euro-Russian heat wave of 2010.* Large parts of eastern Europe and western Russia experienced exceptionally warm conditions during July and August 2010 related to persistent atmospheric blocking, with the most severe impacts over Russia. GHCNDEX indicates strong departures from normal (i.e., the 1961–90 climate average) for most of the temperature indices. For example, over large parts of western Russia, the frequency of warm days (i.e., those above the 90th percentile) in July 2010 was five times higher than the 1961–90 average (Fig. 4a). This was related to record maximum temperatures, the warmest day in July 2010 being more than 5°C warmer than the average warmest July day during 1961–90. Indeed, the area-averaged maximum temperature over western Russia (45°N–65°N, 30°E–55°E) in July 2010 was the highest (area-averaged) July temperature during the entire period covered by GHCNDEX.

*Australian floods of 2010–11.* The El Niño–Southern Oscillation (ENSO) was characterized by ex-
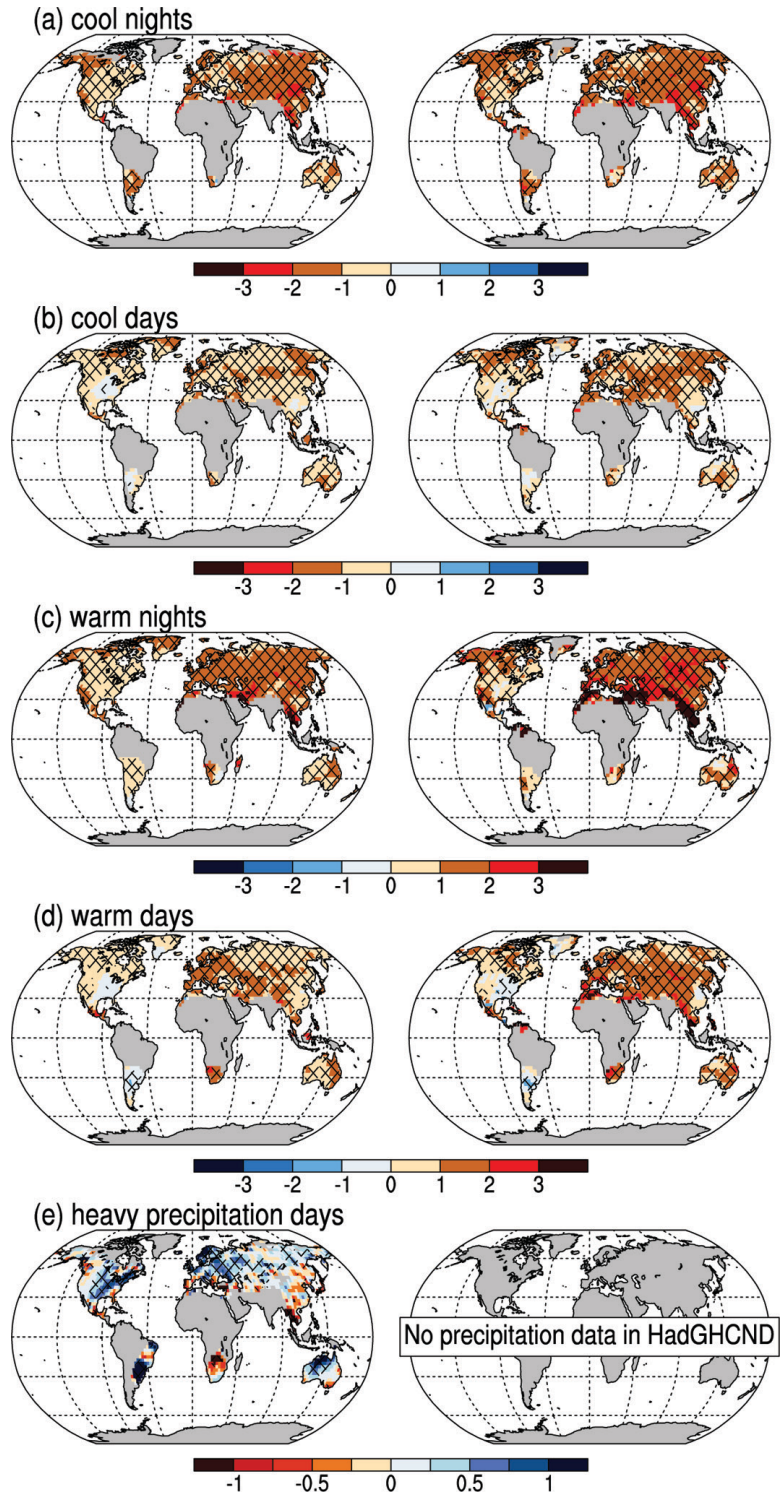


**FIG. 3.** Linear decadal trend estimates (following Sen 1968) for selected extremes indices: (left) GHCNDEX; (right) HadGHCND. Trends are only shown for grid boxes with at least 40 years of data. Hatching indicates significant trends with $p \leq 0.05$ (Mann-Kendall test). Units: (a)–(d) annual % of days per decade; (e) annual number of days per decade.
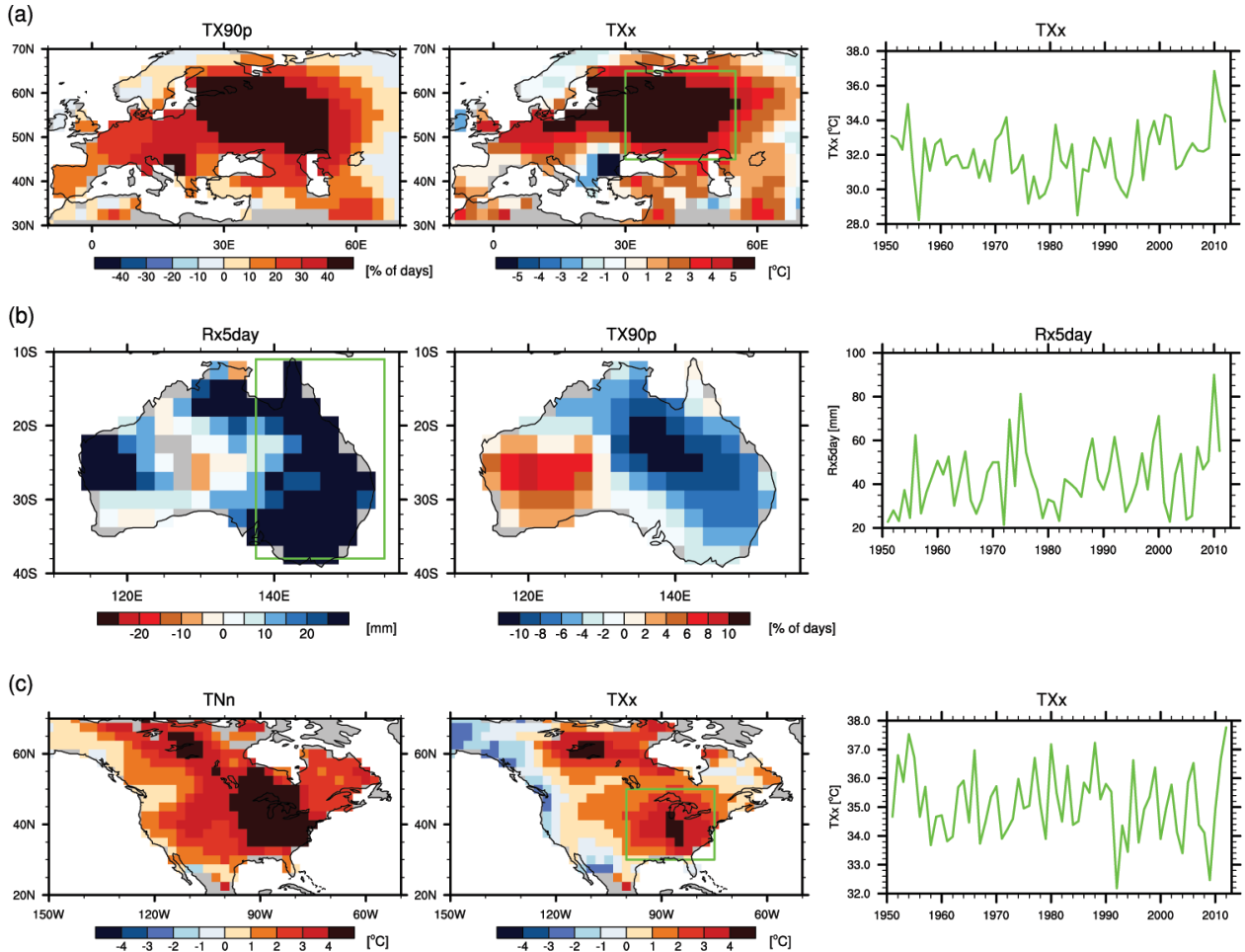
**FIG. 4. Anomalies relative to the 1961–90 climate average of selected indices for three recent extreme events and time series of area-averages for the relevant region. The green boxes indicate the regions for which area-averaged time series are presented. (a) Euro-Russian heatwave of 2010: anomalies of warm days (TX90p) and warmest daily maximum temperature (TXx) during Jul and time series of TXx in Jul, area average for 45°N–65°N, 30°E–55°E; (b) Australian floods of 2010: anomalies of consecutive 5-day precipitation (Rx5day) and warm days (TX90p) and time series of Rx5day during Dec, area average for 38°S–11°S, 137.5°E–155°E; and (c) North American heatwave of 2012: anomalies of coldest daily minimum (i.e., nighttime) temperature (TNn) and warmest daily maximum temperature (TXx) during Jul and time series of TXx in Jul, area average for 30°N–50°N, 100°W–75°W.**

traordinarily strong positive Southern Oscillation index values during the boreal winter in 2011–12, leading to an anomalously wet and cool summer in the eastern part of Australia. This resulted in disastrous flooding in parts of Queensland, while parts of Western Australia were drier and warmer than usual (Fig. 4b). This was reflected by particularly high total precipitation amounts over the entire eastern half of Australia, where an anomalously large number of heavy precipitation days also occurred. In addition, exceptionally high values of 1-day and consecutive 5-day precipitation amounts were ex-

perienced. For example, area-averaged over eastern Australia, the highest consecutive 5-day precipitation amount for December 2010 was higher than in any other December during 1951–2011. Similarly high December precipitation amounts only occurred in 1975. The wet conditions over the eastern part of Australia were accompanied by cooler-than-normal temperatures, as reflected by the reduced number of warm days, for example. The cooling effect of the La Niña conditions is also visible in lower nighttime temperatures, although to a lesser extent than in daytime temperatures.

*North American heatwave of 2012.* Large parts of eastern North America experienced an unusually long period of very high daytime and nighttime temperatures during the 2012 boreal summer. Among the GHCNDEX temperature indices for July of that year, this heat wave is represented by large positive departures from the respective 1961–90 average (Fig. 4c). The largest positive anomalies occurred over the eastern United States, where both the coldest night (TNn), for example, and the highest daily maximum temperature (TXx) were up to 5°C warmer than the 1961–90 average. Averaged over the eastern United States (30°N–50°N, 100°W–75°W), TXx was higher during July 2012 than at any other time since 1951. Strong positive anomalies were also found for the frequency of warm nights and warm days, with values up to four times more frequent than during 1961–90 (not shown). A second center of large positive anomalies in the same temperature indices during July 2012 was located over central Canada.

## WEB-BASED APPLICATION/PRODUCT AVAILABILITY.
The complete suite of datasets related to GHCNDEX, which forms part of a wider project, CLIMDEX, is being made publicly available at www.climdex.org. This includes both the calculated climate indices at all stations and the gridded fields. The website also provides a number of tools to explore the data and to download them in different formats. This enables interested users to investigate the datasets according to their specific needs and also offers transparency toward reproduction of the results.

## CONCLUSIONS.
We present GHCNDEX, a suite of global gridded datasets of climate extremes, which is operationally updated. This enhances previously available climate extremes datasets, which were static in nature. Also, we show good agreement between GHCNDEX and previous datasets with regard to variability and trends in the climate indices. This suggests a robustness of the analyzed changes across different data sources (HadEX) and processing procedures (HadGHCND). With respect to global-scale trends, the main source of differences between the datasets seems to be related to spatial coverage. All data used in the production of GHCNDEX are freely available via the GHCN-Daily archive, which ensures complete reproducibility of the results. However, using only freely available data means that spatial coverage may be more limited in comparison to other complementary datasets that incorporate nonpublic data sources to add spatial coverage in data-sparse regions.

In addition to the presented applications, GHCNDEX may serve as a basis for regional climate change assessments, model evaluation, and detection and attribution studies of changes in climate extremes. As such, it may also be of use for upcoming studies that aim to understand the mechanisms behind the observed changes.

## FOR FURTHER READING

Alexander, L. V., and Coauthors, 2006: Global observed changes in daily climate extremes of temperature and precipitation. *J. Geophys. Res.-Atmos.*, **111**, D05109, doi:10.1029/2005JD006290.

Barriopedro, D. B. D., E. M. Fischer, J. Luterbacher, R. Trigo, and R. Garcia-Herrera, 2011: The hot summer of 2010: Redrawing the temperature record map of Europe. *Science*, **332**, 220–224.

Caesar, J., L. Alexander, and R. Vose, 2006: Large-scale changes in observed daily maximum and minimum temperatures: Creation and analysis of a new gridded data set. *J. Geophys. Res.*, **111**, D05101, doi:10.1029/2005JD006280.

Donat, M. G., and Coauthors, 2012: Updated analyses of temperature and precipitation extreme indices since the beginning of the twentieth century: The HadEX2 dataset. *J. Geophys. Res.*, **118**, 2098–2118.

Durre, I., M. J. Menne, B. E. Gleason, T. G. Houston, and R. S. Vose, 2010: Comprehensive automated quality assurance of daily surface observations. *J. Appl. Meteor. Climatol.*, **8**, 1615–1633.

Kendall, M. G., 1970: *Rank correlation methods*. 4th ed. Charles Griffin, 202 pp.

Matsueda, M., 2011: Predictability of Euro-Russian blocking in summer of 2010. *Geophys. Res. Lett.*, **38**, L06801, doi:10.1029/2010GL046557.

Menne, M. J., I. Durre, B. G. Gleason, T. G. Houston, and R. S. Vose, 2012: An overview of the Global Historical Climatology Network-Daily database. *J. Atmos. Oceanic Technol.*, **29**, 897–910.

National Climate Centre, Bureau of Meteorology, 2011: Frequent heavy rain events in late 2010/early 2011 lead to widespread flooding across eastern Australia. Special Climate Statement 24, 28 pp. [Available online at http://reg.bom.gov.au/climate/current/statements/scs24c.pdf.]

Pan, Z., R. W. Arritt, E. S. Takle, W. J. Gutowski Jr., C. J. Anderson, and M. Segal, 2004: Altered hydrologic feedback in a warming climate introduces a "warming hole." *Geophys. Res. Lett.*, **31**, L17109, doi:10.1029/2004GL020528.

Peterson, T. C., and M. J. Manton, 2008: Monitoring changes in climate extremes: A tale of international collaboration. *Bull. Amer. Meteor. Soc.*, **89**, 1266–1271, doi:10.1175/2008BAMS2501.1.

Portmann, R. W., S. Solomon, and G. C. Hegerl, 2009: Spatial and seasonal patterns in climate change, temperatures, and precipitation across the United States. *Proc. Natl. Acad. Sci. USA*, **106**, 7324–7329, doi:10.1073/pnas.0808533106.

Sen, P. K., 1968: Estimates of the regression coefficient based on Kendall's Tau. *J. Am. Stat. Assoc.*, **63**, 1379–1389.

Shepard, D., 1968: A two-dimensional interpolation function for irregularly spaced data. *Proc., 23rd Association for Computing Machinery National Conference*, 517–523.

## ECHOES

" **We think this discovery is a game-changer in the world of alternative energy."**

—Virginia Tech Professor Y. H. Percival Zhang, speaking about new research in which he and colleagues were able to produce large amounts of high-quality hydrogen from plants with almost no release of greenhouse gases through the use of xylose, the second-most common sugar found in plants. The scientists extracted enzymes from a number of different microorganisms, then added xylose and a polyphosphate to create a reaction that not only releases the hydrogen from the xylose in amounts three times greater than other hydrogen-producing microorganisms but also does so at a relatively low temperature (122°F) and under normal atmospheric pressure. The new method is highly efficient and results in a net energy gain— something that is not possible with other processes that convert sugar into biofuels such as ethanol and butanol. The research, which was recently published in the online version of *Angewandte Chemie, International Edition*, "could help end our dependence on fossil fuels," according to Zhang. (Source: Virginia Tech)